Supplementary Information for "Constructing the Equilibrium Ensemble of Folding Pathways from Short Off-Equilibrium Simulations"

Frank Noé [*] [†], **Christof Schütte** [*], **Eric Vanden-Eijnden** [‡], **Lothar Reich** [§], **and Thomas R. Weikl** [§]

[*]DFG Research Center Matheon, FU Berlin, Arnimallee 6, 14195 Berlin, Germany,[†]Correspondance to: frank.noe@fu-berlin.de,[‡]Courant Institute, New York University 251, Mercer street, New York, NY, 10012, and [§]Max Planck Institute for Colloids and Interfaces, Science Park Golm, 14424 Potsdam, Germany

Submitted to Proceedings of the National Academy of Sciences of the United States of America

Model System Setup. The model system (Fig. 2 in the paper) used to illustrate transition path theory, has been set up in the following manner. First, a potential function was set up as:

$$\begin{aligned} V(x,y) &= x^2+y^2-50\cos\sqrt{\left(\frac{x-25}{1.7}\right)^2+\left(\frac{y-25}{1.7}\right)^2} \\ &\quad -50\mathcal{N}(x,y,20,20,4,4) \\ &\quad -30\mathcal{N}(x,y,30,30,8,3) \\ &\quad -70\mathcal{N}(x,y,7,25,4,15) \\ &\quad -40\mathcal{N}(x,y,25,7,15,4) \\ &\quad -50\mathcal{N}(x,y,40,40,3,3) \end{aligned}$$

with Gaussian-type energy basins defined as

$$\mathcal{N}(x,y,\mu_x,\mu_y,\sigma_x,\sigma_y)=\exp\left(-\frac{(x-\mu_x)^2}{\sigma_x^2}-\frac{(y-\mu_y)^2}{\sigma_y^2}\right)$$

The potential $V(x,y)$ was then evaluated on a lattice of x,y integer values in the range 0,...,49. On this lattice, a jump process was defined by a transition matrix with each row corresponds to one coordinate x,y and is defined by

$$\begin{aligned} T_{x,y\to x,y} &= z^{-1} \\ T_{x,y\to x,y-1} &= z^{-1}\min\{1,\exp[-\beta(V(x,y-1)-V(x,y))]\} \\ T_{x,y\to x,y+1} &= z^{-1}\min\{1,\exp[-\beta(V(x,y+1)-V(x,y))]\} \\ T_{x,y\to x-1,y} &= z^{-1}\min\{1,\exp[-\beta(V(x-1,y)-V(x,y))]\} \\ T_{x,y\to x+1,y} &= z^{-1}\min\{1,\exp[-\beta(V(x+1,y)-V(x,y))]\} \end{aligned}$$

where z is chosen such that the transition matrix row sums up to 1. Entries that would go across the 0,...,49 boundary, such as $T_{0,0\to 0,-1}$ are forced to zero. This dynamics is a Monte Carlo jump process on a discrete lattice with potential defined by $V(x,y)$.

The sets A and B were defined by all lattice points that are inside a radius of 6 and outside a radius of 16 from the center at (25,25).

Since the dynamics is Markovian by definition, the application of transition path theory consisting of computation of the stationary probability, the committor probabilities, the folding flux and the coarse-grained folding flux, is exact.

PinWW Simulation Setup. All simulations were carried out with the 3.2.1 version of the GROMACS engine [1] using the GROMOS-96 43a1 force field. LINCS constraints [2] of order 4 using a tolerance of 10^{-4} nm were applied to all bond lengths (see also [14]) and masses of heavy atoms were redistributed such as to increase the masses of covalently bound hydrogen atoms to 4 atomic mass units [15]. This permitted an integration time step of 4 fs [16]. Van der Waals interactions were considered within a twin range cutoff of 0.8 and 1.4 nm without inclusion of long-range dispersion corrections so as to be consistent with the way the force field was parametrized [17]. The reaction field method was chosen to calculate electrostatic interactions. The Coulomb potential was cutoff at 1.4 nm. The dielectric constant of the continuum was set to 54 so as to be consistent with the SPC water model that was used in the simulations [3]. Both temperature and pressure were controlled with the Berendsen scheme, the coupling constants being 0.1 ps and 1 ps respectively. The pressure was kept at 1 bar and the compressibility of the system at 5×10^6 bar.

The crystal structure of the Pin1WW domain (pdb code 1pin, residues 6 to 39) [4] was centered in an octahedral simulation box with at least 1.2 nm distance between the protein and the box walls and subsequently solvated with SPC water. The positive net charge in the protein was neutralized by the addition of four chloride ions to the system. Energy minimization was performed by 2000 steps of the steepest descent algorithm followed by an equilibration phase of 900 ps at 300 K while restraining positions of protein atoms by a harmonic potential with force constant 1000 kJ mol^{-1} nm^{-2}. Four 80 ns simulations at 300 K were started from the equilibrated structure using different initial velocities drawn from the Maxwell-Boltzmann distribution. A structure every 3.2 ns was extracted from these trajectories, providing a total of 100 near-native structures. These structures were used as starting structures for 100 simulations of 115 ns at 360 K. From the resulting ensemble, 80 structures were chosen randomly, again starting simulations of 115 ns each at 360 K. Output was written every 4 ps, resulting in a set of 5,175,000 configurations from the 360 K simulations used in the analysis below.

Markov model building, validation and uncertainty. The following steps were taken towards computing a Markov state model for the PinWW simulations. All configurations were aligned to the X-ray structure *via* a root-mean-square deviation fit on the backbone atoms in order to remove translation and rotation of the whole system. The k-means algorithm was run to convergence to generate 3000 clusters using Euclidean distances in the Cartesian coordinates of all atoms, thus providing a fine partition of state space into conformational states. This fine partition is necessary in order to avoid that different metastable sets are lumped in single clusters. Each configuration that was saved from the simulation trajectories was then mapped onto the cluster it is located in, obtaining 180 discrete-state trajectories of 115 ns each amongst the conformational states. In order to obtain a good Markov model of the molecular dynamics that has no significant bias and known statistical uncertainties, the following steps were taken:

Reserved for Publication Footnotes

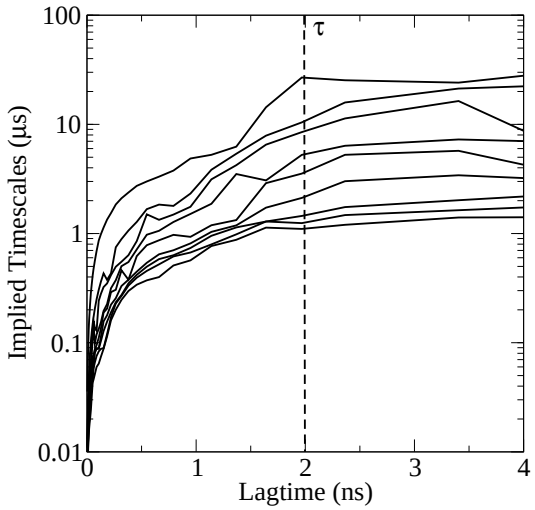

Figure 1. Implied timescales depending on the lagtime τ.

1. Statistically unreliable states that would bias the Markov model towards spurious kinetics are identified and excluded from the analysis.
2. The lagtime τ at which the state-to-state dynamics becomes approximately Markovian was computed.
3. The maximum likelihood estimates for the transition probabilities between all pairs of states, $T_{ij}(\tau)$, are computed while assuring that these estimates have no significant bias from the way trajectories were launched.
4. It is tested whether the resulting model fulfills $\mathbf{T}(n\tau) \approx \mathbf{T}^n(\tau)$ by comparing $p(t + n\tau) = p(t)\mathbf{T}(n\tau)$ obtained from the molecular dynamics simulations to $p(t)\mathbf{T}^n(\tau)$ computed from the Markov model.
5. It is tested whether consistent models can be built from two subsets of the data with different trajectory starting conditions.
6. The statistical uncertainties of the resulting model $\mathbf{T}(\tau)$ and the properties computed from it are estimated.

As a first step, it is necessary to avoid incorporating pathological states, including states that are extremely rarely visited, or sets of states that are never left since they e.g. only occur at the end of one of the trajectories. Therefore, only clusters were kept if they were observed in at least 0.01 % of the available configurations. Subsequently, only those clusters were used for the analysis which were in the largest connected subnetwork, where two states $i \to j$ are connected if a transition $i \to j$ has been observed in any trajectory. The remaining data were ignored as their inclusion into the model would have caused numerical artifacts in the computation of the transition matrix. In the subsequent analysis, transitions between states were only counted for trajectory segments that stay within the set of maintained states.

Secondly, for the remaining 1734 clusters, transition matrices $\mathbf{T}(\tau)$ with different values of the lagtime τ were computed. In order to choose a lagtime at which the dynamics is approximately Markovian for this definition of states, the approach suggested in [5] was followed: For each lagtime τ, the transition matrix $\mathbf{T}(\tau)$ and the timescales implied by its eigenvalues λ_i, $t_i = -\tau/\log(\lambda_i)$, were computed (see Fig. 1. At $\tau \approx 2$ ns these timescales become approximately constant, indicating Markovianity at that or longer timescales. Thus, $\tau = 2\text{ns}$ was used for the Markov model here.

Thirdly, the transition probability for each transition $i \to j$ (corresponding to conformation sets Ω_i and Ω_j within time step τ is theoretically given by

$$T_{ij} = \int_{x \in \Omega_i} \pi_i(x)\, p(x, \Omega_j, \tau),$$

where π_i is the stationary density restricted to set Ω_i and $p(x, \Omega_j, \tau)$ is the probability of finding the system in Ω_i a time τ after observing it at x. While any trajectory segment of length τ can be used to give an unbiased sample of $p(x, \Omega_j, \tau)$, their starting points need to be drawn from the local equilibrium $\pi_i(x)$ such that the estimator

$$\hat{T}_{ij} = \frac{c_{ij}(\tau)}{\sum_k c_{ik}(\tau)}$$

with c_{ij} being the number of observed $i \to j$ transitions in time τ provides an unbiased sample of $T_{ij}(\tau)$. For trajectories that are much longer than the local equilibration time of the states i, only a small segment at the beginning of the trajectory could be biased by an off-equilibrium starting condition. After that, the trajectory will sample from the local equilibria as it passes through the states. To estimate the local equilibration times, following procedure was employed: Each of the 1734 states, was further partitioned into 2 substates, and the 2×2-transition matrix between them was computed at a lag time of 2 ns. The second eigenvalue, λ_2, provides the slowest timescale of that sub-transition matrix via $t_{\text{relax}} = -\frac{2\text{ ns}}{\log \lambda_2}$, which is an estimate for the relaxation time within the corresponding cluster. For the present case, all t_{relax} of trajectory starting states were below 1 ns, most of them were around 0.5 ns. This indicates that within the lag time used of 2 ns, the bias due to the starting condition should be even small for the first transition observed in a trajectory. Each trajectory has a length of 115 ns, while the lag time is 2 ns. Thus, even if the first 2.5 independent transition events (≥ 5 relaxation times) are somewhat affected by the off-equilibrium starting conditions, this will only mean that 5% of the transition counts are sampled with a bias.

As a fourth step, note that observing the implied timescales to select an appropriate value of τ and finding that the transition matrix can be estimated in a nearly unbiased fashion from the trajectory at that lag time, are both not rigorous tests of whether the obtained model $\mathbf{T}(\tau)$ is a good model of the long-time dynamics. Therefore, it was also tested whether the Markov model can reproduce the statistics of the molecular dynamics simulation by observing the time-dependent probabilities in following sets

1. The folded set B, which are all clusters with mean rmsd to the X-ray structure of less than 0.3 nm
2. The unfolded set A, which are all clusters with an average of less than 3 hydrogen bond in hairpin 1 and less than 1 hydrogen bond in hairpin 2.
3. 10 random sets C_i obtained by partitioning state space randomly into 10 sets such that each set is contiguous (i.e.: states in each set are connected by a series of direct jumps in the trajectories without having to cross another set).

Let $s_k(t) \in \{1, ..., m\}$ denote the state history of the k'th trajectory, then the probability distribution of finding a state i in the trajectory data is given by

$$w_i = \frac{\sum_{k=1}^{n} \sum_{t=1}^{T_k} \delta(s_k(t) - i)}{\sum_{k=1}^{n} T_k}$$

where T_k is the length of the kth trajectory and $\delta(x) = 1$ for $x = 0$ and 0 for all other x. The probability restricted to a set C is then given by

$$w_i^C = \begin{cases} \frac{w_i}{\sum_{j \in C} w_j} & i \in C \\ 0 & i \notin C \end{cases}.$$

As a model test, the following "relaxation experiment" was carried out for each set: Using w_i^C as initial probability for each of the sets under consideration (A, B, C_i), the probability of being at that set at later times $r\tau$ was then computed according to (i) the molecular dynamics trajectories and (ii) the Markov model, and subsequently

compared. The time-dependence of the probability to be at set C with starting distribution w_i^C is given by:

$$p_{\mathrm{MD}}(C,C,r\tau) = \frac{\sum_{i\in C}\ w_i^C\ p_{\mathrm{MD}}(i,C,r\tau)}{\sum_{i\in C}\ w_i^C}$$

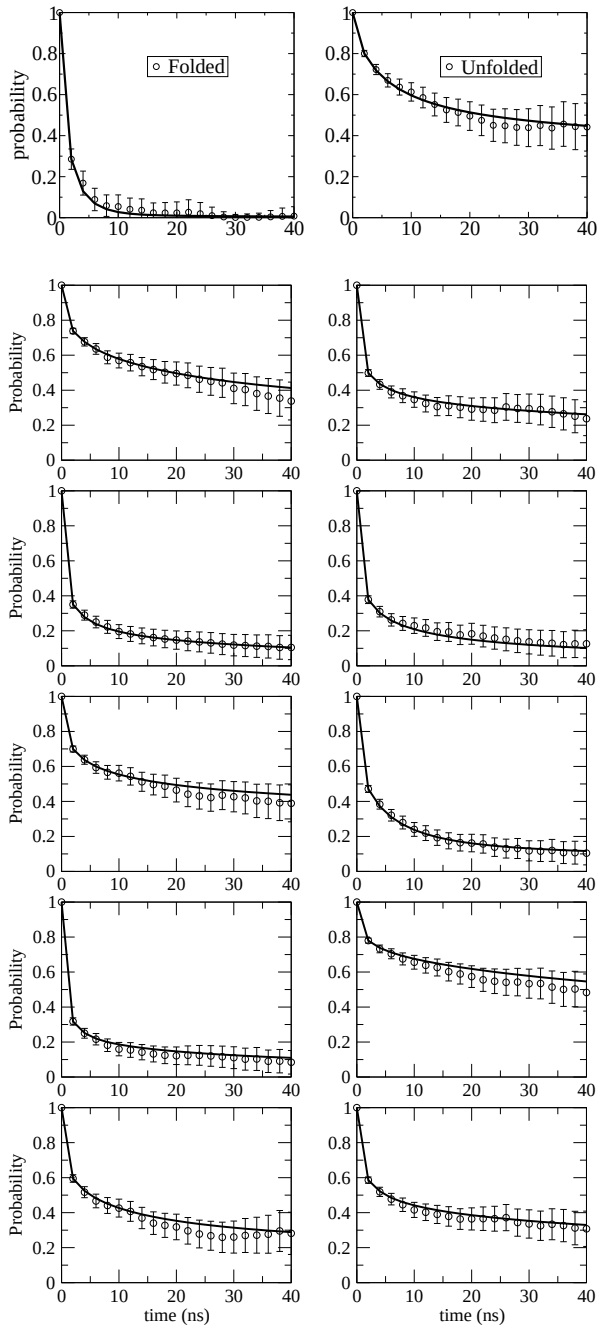

Figure 2. Markov model test: The validity of the Markov model (solid line) is compared with the MD trajectories (bullets) by monitoring the relaxation of probability out of different sets of states. Top two panels: Folded set B and Unfolded set A. Bottom ten panels: The state space is partitioned randomly into 10 contiguous sets.

with

$$\begin{aligned} &p_{\mathrm{MD}}(i,C,r\tau) \\ &= \frac{\sum_{k=1}^{n}\sum_{t=1}^{T_n-r\tau}\sum_{j\in C}\delta(s_k(t)-i)\,\delta(s_k(t+r\tau)-j)}{\sum_{k=1}^{n}\sum_{t=1}^{T_n-r\tau}\delta(s_k(t)-i)} \\ &= \frac{\sum_{j\in C}\ c_{ij}(r\tau)}{\sum_{j=1}^{m}\ c_{ij}(r\tau)}, \end{aligned}$$

with $c_{ij}(r\tau)$ being the number of transitions $i \rightarrow j$ observed after time lag $r\tau$.

Likewise, the probability to be at C according to the Markov model is given by:

$$p_{\mathrm{MSM}}(C,C,r\tau) = \sum_{i\in C}[w^C\ \mathbf{T}^{\mathbf{r}}(\tau)]_{\mathbf{ii}}.$$

Testing the validity of the Markov model then amounts to testing how well the equality

$$p_{\mathrm{MD}}(C,C,r\tau) = p_{\mathrm{MSM}}(C,C,r\tau) \qquad \textbf{[1]}$$

holds, which is essentially a test of the Chapman-Kolmogorow property. Note that the initial distribution w_i^C is simply a reference distribution with respect to which the comparison is made. Instead, other distributions could be used, such as the stationary distribution induced by the Markov model $\mathbf{T}(\tau)$ restricted to set C.

The equality (1) is not expected to hold exactly as a result of statistical uncertainties caused by the fact that only a finite number of transitions are available to estimate the true transition probabilities. In order to take this into account, the uncertainties of the transition probabilities estimated from the molecular dynamics trajectories are computed as:

$$\begin{aligned} \epsilon(A,A,r\tau) &= \sigma[p(i,A,r\tau)]\sqrt{\frac{r}{\sum_{j=1}^{m}c_{ij}(r\tau)}} \\ &= \sqrt{\frac{r(p(i,A,r\tau)-p^2(i,A,r\tau))}{\sum_{j=1}^{m}c_{ij}(r\tau)}}, \end{aligned}$$

where σ indicates the standard deviation. The test then consists of assessing whether Eq. (1) holds within these uncertainties. Fig. 2 shows this comparison for sets (A, B, C_i), showing the the Markov model excellently reproduces the observations of the molecular dynamics trajectories within the statistical uncertainties. This test was

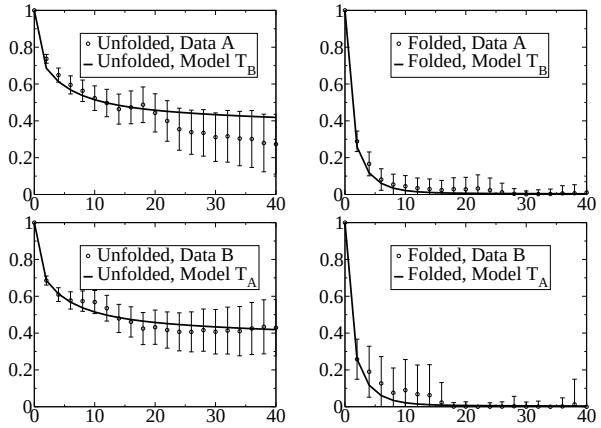

Figure 3. Cross-validation of two subsets of the data. Subset A consisted of 70% of the trajectories started from the folded state and 30% other trajectories. Subset B contained the remaining 30%/70% of the trajectories. The Markov models $\mathbf{T}_A$ and $\mathbf{T}_B$ were built out of data sets A and B, respectively. The figure shows that data set A is consistent with model $\mathbf{T}_B$ and vice versa.

repeated multiple times with different random sets C_i, and always led to a similar agreement.

As a fifth step, a cross-validation between two subsets of the data was conducted in order to further reduce the risk that the model was significantly biased by the starting points of the trajectories. For this, the data was subdivided into two sets:

1. Data set (A) contains 70% of the trajectories started from the native state and 30% of the other trajectories. A Markov model $\mathbf{T}_A$ was constructed only from this data set in otherwise the same way as $\mathbf{T}$.
2. Data set (B) contains the remaining 30% of the trajectories started from the native state and the remaining 70% of the other trajectories. A Markov model $\mathbf{T}_B$ was constructed only from this data set

Two Chapman-Kolmogorov tests as described above were then conducted, now comparing data set (A) with model $\mathbf{T}_B$ and data set (B) with model $\mathbf{T}_A$. These tests showed that both models and data sets are compatible within statistical error. The results for the folded and unfolded sets are shown in Fig. 3.

Due to the fact that the Markov model is always constructed with only a finite amount of simulation data, all properties computed from the model will have statistical uncertainties associated with them. A flexible and general method to compute uncertainties of the Markov model and all the properties computed from it is to sample transition matrices according to their probability distribution induced by the observed count matrix $\mathbf{C} = [\mathbf{c_{ij}}]$ [12, 13]:

$$p(\mathbf{T} \mid \mathbf{C}) \propto p(\mathbf{T}) p(\mathbf{C} \mid \mathbf{T})$$

Using a Dirichlet-form prior distribution, this can be rewritten as [12, 13]:

$$p(\mathbf{T} \mid \mathbf{C}) \propto \prod_{i,j=1}^{m} (T_{ij})^{b_{ij}-1+c_{ij}} \qquad \textbf{[2]}$$

where b_{ij} are virtual prior counts that can be e.g. set to 1 if an a priori uniform distribution of transition matrix elements is desired [13] or to a constant n/m with some $n \geq 0$ which guarantees that there is a constant number of n prior counts in each row, independent how many states are used to discretize the system [12]. Here, we used no prior counts $n = 0$, thus giving the prior minimal and the actual observations maximal impact. For the present 1734 state model this prior is almost identical to the $1/m$ prior suggested in [12] with the additional nice property that the probability distribution in Eq. (2) is always unimodal. To sample the resulting distribution (2), the nonreversible transition matrix sampling algorithm described in [13] was applied. Starting from the maximum likelihood transition matrix $t_{ij} = c_{ij} / \sum_k c_{ik}$, 10^9 Monte-Carlo steps were taken to generate a well-mixed ensemble of transition matrices, and every 10^6th matrix was used to compute the property of interest (TPT net fluxes, cumulative fluxes, timescales). The 80% confidence intervals centered on the mean was computed for each of these resulting ensembles in order to provide uncertainty intervals.

Coarse-Graining. In order to present a coarse-grained visualization of the flux, the state space must be partitioned into meaningful coarse sets. From a kinetic point of view, it is desirable to do this partitioning according to the metastabilities in the system, that is for a given timescale of interest, those states will be grouped together which interconvert rapidly within this timescale, while states which do not interconvert rapidly are separated into different metastable sets. A method to do this is the Perron cluster analysis (PCCA) [6, 7, 8], applied here. First, the timescales $t_i = -\tau / \log(\lambda_i)$ implied by the eigenvalues λ_i of the transition matrix $\mathbf{T}(\tau)$ are inspected. Based on this relation, one can select a timescale of interest and thus obtains the number of eigenvalues, and thus metastable states, the system decomposes into. In the present system, 41 metastable states exist on a timescale of 100 ns. The definition of these 41 metastable states in terms of the conformational states $\{1, ..., m\}$ they contain is obtained from a clustering in the eigenvector space, as defined by the PCCA method [6, 7, 8]. In the original PCCA method [6], the m conformational states are assigned to M metastable states according to the sign structure of the corresponding elements in the M first right eigenvectors of $\mathbf{T}(\tau)$. In the improved PCCA method [7] used here, this clustering is made by first identifying M "vertices" in the $M-$dimensional eigenvector space, which are the most distant elements in this space and correspond to M representative conformational states of the metastable states. Subsequently, all other $m - M$ conformational states are assigned to the metastable sets with the nearest representative.

Some of the resulting 41 metastable sets contain conformational states from both A and I or both B and I, i.e. coarse-graining the folding flux onto them would destroy the definition of the unfolded set A and the folded set B. Therefore, these states were split into two substates, each containing only A, B or I states. As a result, 50 macrostates are obtained which were used to coarse-grain the folding flux as described in the Theory section.

Transition Path Theory with derivations. We first derive the forward committor probability for a Markov chain defined on state space $S = 1, ..., m$. We define the source set A, the target set B, and the intermediate set I. The committor probability, q_i^+ pertaining to two sets A, B is the probability that starting in state i, we will go to B next rather than to A. In order to compute this, we define an A-absorbing process as

$$\hat{T}_{ij} = \begin{cases} T_{ij} & i \notin A \\ 1 & i \in A, i = j \\ 0 & i \in A, i \notin j \end{cases}$$

and then compute q^+ as the hitting probability to B (see [9]). Since the process is absorbing in A only, the hitting probability to B will reflect the probability to go to B next rather than to A. This yields:

$$\begin{aligned} q_i^+ &= 0 \ \text{ for } i \in A \\ q_i^+ &= 1 \ \text{ for } i \in B \\ q_i^+ &= \sum_{j \in S} T_{ij} q_j^+ \ \text{ for } i \notin \{A, B\}. \end{aligned}$$

One only needs to solve q_i for $i \notin \{A, B\}$, and by incorporating the constraints from the first two lines into the third line, one obtains:

$$-q_i^+ + \sum_{k \in I} T_{ik} q_k^+ = -\sum_{k \in B} T_{ik} \ \text{ for } i \in I.$$

While $\mathbf{T}(\tau)$ models the dynamics of the system forward in time, one can likewise define a transition matrix $\tilde{\mathbf{T}}(\tau)$ propagating the dynamics backward in time. This backward transition matrix is defined as: $\tilde{T_{ij}} = \frac{\pi_j}{\pi_i} T_{ji}$ [9]. In a similar way as the forward committor, one obtains the backwards committor q^- as:

$$-q_i^- + \sum_{k \in I} \tilde{T}_{ik} q_k^- = -\sum_{k \in A} \tilde{T}_{ik} \ \text{ for } i \in I.$$

If the system fulfills detailed balance, we have $\pi_i \tilde{T}_{ij} = \pi_j \tilde{T}_{ji}$ and thus $q^+ = 1 - q^-$.

The flux along each $i \to j$ pair is defined as

$$f_{ij}^{AB} = \begin{cases} \pi_i q_i^- T_{ij} q_i^+ & i \neq j \\ 0 & i = j \end{cases}.$$

The total amount of flux, F, that leaves states A will enter B:

$$F := \sum_{a \in A, j \notin A} f_{aj} = \sum_{j \notin A, b \in B} f_{jb}$$

and all other states are flux-conserving:

$$\sum_{j=1\ldots m} (f_{ij}^{AB} - f_{ji}^{AB}) = 0 \quad \forall i \notin \{A, B\}$$

Proof:

$$\begin{aligned}\sum_{j=1\ldots m} (f_{ij}^{AB} - f_{ji}^{AB}) &= \pi_i q_i^- \sum_{j\neq i} T_{ij} q_j^+ - q_i^+ \sum_{j\neq i} \pi_j q_j^- T_{ji} \\ &= \pi_i q_i^- \sum_{j\neq i} T_{ij} q_j^+ - \pi_i q_i^+ \sum_{j\neq i} q_j^- \tilde{T}_{ij}\end{aligned}$$

Due to the committor equations, we can rewrite $\sum_{j\neq i} T_{ij} q_j^+$ as $-T_{ii} q_i^+$ and $\sum_{j\neq i} \tilde{l}_{ji} q_j^-$ as $-\tilde{T}_{ii} q_i^-$ and thus:

$$\sum_{j=1\ldots m} (f_{ij}^{AB} - f_{ji}^{AB}) = -\pi_i q_i^- T_{ii} q_i^+ + \pi_i q_i^+ \tilde{T}_{ii} q_i^- = 0.$$

From $q_i^+ = 1$ for $i \in A$ and $q_i^- = 0$ for $i \in B$ we see that

$$\begin{aligned} f_{ij}^{AB} &= 0 \text{ for } j \in A \\ f_{ij}^{AB} &= 0 \text{ for } i \in B \end{aligned}$$

thus flux is not conserved at A and B, but throughout the network such that:

$$\sum_{i\in A, j\notin A} f_{ij}^{AB} = \sum_{j\notin B, i\in B} f_{ji}^{AB}.$$

Note that the total flux, F, yields the expected number of observed $A \to B$ transitions per time unit τ. This number is affected by the fact that the system, after having committed to B, needs first to get back to A before being able to conduct another $A \to B$ transition. In order to compute rates, we also need the total probability that the system is on a "forward" move, i.e. that it had been in A last is given by:

$$\pi_A = \sum_{i=1}^{m} \pi_i q_i^- .$$

Thus, the probability of a productive trajectory given that the system had visited A last is given by F/π_A while the corresponding $A \to B$ transition rate is given by

$$k_{AB} = \frac{F}{\tau \pi_A}.$$

Finally, the net flux is defined as

$$f_{ij}^+ = \max\{f_{ij}^{AB} - f_{ji}^{AB}, 0\}$$

and inherits the flux conservation property from the reactive flux.

The resulting folding flux can be decomposed into individual pathways. While various ways are available to do this, a particularly interesting approach is to identify the strongest pathways first and iteratively remove them from the network until the network is entirely decomposed, as described in [10]. Roughly, the algorithm proceeds as follows.

1. $D = \emptyset$.
2. Let $P = \{p_1 \in A, p_2, ..., p_{l-1}, p_l \in B\}$ be the pathway with the greatest minimal flux f.
3. For $j = 1...(l-1)$
3.1. $f^+_{p_j p_{j+1}} := f^+_{p_j p_{j+1}} - f$
4. Add $\{P, f\}$ to D.
5. If no $A \to B$ pathway exists, return D. Otherwise go to 2.

Comparison of Model and Experiment. The temperature-dependent probabilities of being in the denatured state are determined in [11] by melting curves using UV CD and Tryptophan (Trp) fluorescence spectroscopy. The probability is given relative to the baselines obtained at low and high temperatures. For T=360 K, we obtain from Eq. (2) with the parameters from Table 2 in Ref. [11] $\Delta G = 14.1$ kJ mol^{-1} and thus $p_{\mathrm{folded}} = 0.009$. Since in the present simulation only one temperature is available, and the observables UV CD or Trp fluorescence cannot be precisely computed, this figure cannot be directly compared to the present model. However, we can ask how close we need to be to the native state in order to have a similar probability of being native. $p_{\mathrm{folded}} = 0.009$ corresponds to the set of all structures within 0.3 nm of the native state, which is a reasonable definition for "native". It was also found that the probability of being folded is rather robust and below 5% when including structures up to about 0.5 nm of the X-ray structure. Thus, independent of the exact definition of "native", simulation model and experiment agree that the PinWW structure is mostly unfolded at 360 K.

In [11], temperature jump experiments were conducted using the intrinsic PinWW Trp fluorescence as indicators. For this, the fluorescence decay curve at any time t, $f(t)$ was compared to the fluorescence decay curves at the elevated temperature, f_D, ("denatured") and the one at the final temperature, f_N, ("native"), by determining the linear combination:

$$f(t) = a_D(t)\, f_D + a_N(t)\, f_N.$$

The factors a_D and a_N determine the percentage of the ensemble being relaxed from the elevated to the equilibrium temperature via:

$$\chi(t) = \frac{a_D(t)}{a_D(t) + a_N(t)}. \qquad \textbf{[3]}$$

Trp fluorescence is modulated by the polarizability of the solvating groups. Thus, the solvent-accessible surface area (SASA) is a good indicator for the fluorescence state of a Trp. Here, two Trp residues, Trp11 and Trp34, are available. The SASA was computed for each of them for each molecular dynamics frame. The mean Trp SASA for Trp11 for any conformational state i is then given by:

$$s_{11,i} = \frac{\sum_k X_i(k) s_{11}(k)}{\sum_k X_i(k)},$$

where $X_i(t)$ is 1 if the tth frame is in state i and 0 otherwise. Analogous for Trp34 and $s_{34,i}$. To simulate the relaxation of the ensemble out of equilibrium to the present simulation temperature of 360 K, we started with a uniform probability distribution, $\mathbf{p}(0) = [m^{-1}, ..., m^{-1}]^T$, which was propagated using the transition matrix:

$$\mathbf{p}(\mathbf{t} + \tau) = \mathbf{p}(\mathbf{t})\mathbf{T}(\tau)$$

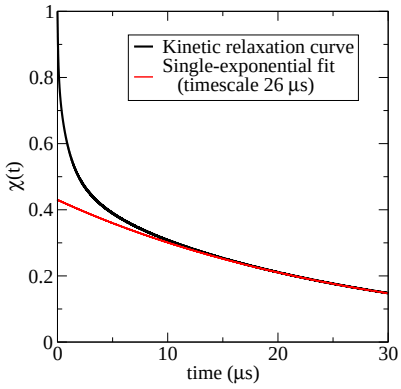

Supplementary Figure 5

Figure 4. Kinetic relaxation of Trp SASA upon refolding.

towards the equilibrium distribution. The SASA-values at any time were computed as ensemble average:

$$s_{11}(t) = \sum_{i=1}^{m} p_i(t)\, s_{11,i}$$
$$s_{34}(t) = \sum_{i=1}^{m} p_i(t)\, s_{34,i},$$

and the factors a_D and a_N were computed analogously to the interpolated fluorescence relaxation curve in the experiment *via*:

$$\begin{pmatrix} s_{11}(t) \\ s_{34}(t) \end{pmatrix} = a_D(t) \begin{pmatrix} s_{11}(\infty) \\ s_{34}(\infty) \end{pmatrix} + a_N(t) \begin{pmatrix} s_{11}(0) \\ s_{34}(0) \end{pmatrix}$$

and the percentage of being relaxed, $\chi(t)$, was computed using Eq. (3). The relaxation curve is plotted in Fig. 4b. There is an initial nonexponential relaxation towards a value of ≈ 0.4 after ≈ 5 μs followed by a single-exponential relaxation with a timescale of 26 μs. Similarly, the experiment shows a fast nonexponential relaxation to a value of ≈ 0.4, followed by a single-exponential relaxation with a timescale of $\approx$13.2 μs [11] (obtained from the kinetic parameters given in Table 3 of Ref. [11] and the Arrhenius prefactor used there).

While the relative intensity of the slowest exponential relaxation (0.4) depends somewhat on the definition of the starting distribution and the way how Trp fluorescence is measured in the model, the timescale itself is insensitive to these definitions as it is determined by the slowest timescale implied by the transition matrix $\mathbf{T}(\tau)$ and thus defined by the second eigenvalue. Thus, the Markov model agrees well with available experimental data.

Projection of Observables onto the committor. Expectation values of observables o may be monitored along the folding transition by projecting them onto q^+:

$$\bar{o}(q,\Delta) = \frac{\sum_{\{i|q_i^+ \in [q-\Delta, q+\Delta]\}} \pi_i o_i}{\sum_{\{i|q_i^+ \in [q-\Delta, q+\Delta]\}} \pi_i}.$$

where Δ is a bin width that is necessary since there are only finitely many states i, o_i is the average of the observable in state i and π_i is the stationary distribution of state i. Fig. 5a-c show how the number of h-bonds in the two hairpins evolve along the folding coordinate. The sum of both hairpin h-bonds (panel c) shows a roughly monotonous increase in two subsequent steps at $q^+ = 0.1$ and at $q^+ = 0.5$. However, looking at the two hairpins individually (panels a and b), shows a much more complex situation: In the range $q^+ = 0.1...0.5$, both hairpins form and break in an approximately anticorrelated way. Hairpin 2 is the first to stably form, hairpin 1 follows after $q^+ = 0.5$. This apparently complicated behavior can be the result of different pathways with different individual mechanisms overlapping in the q^+ coordinate. In general, the projection onto a single degree of freedom reduces the information available in the full-dimensional space and may thus be deceptive if one is interested in kinetic information.

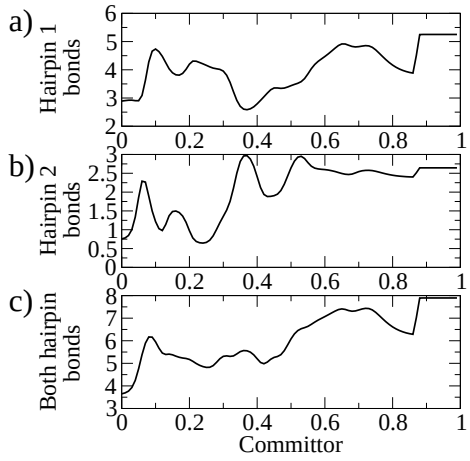

Supplementary Figure 4

Figure 5. Expected number of β-hairpin hydrogen bonds formed along the committor probability (p_{fold}).

1. van der Spoel et al. (2005) GROMACS: Fast, Flexible and Free. *J Comput Chem* 26:1701–1718.
2. Hess, B, Bekker, H, Berendsen, HJC, Fraaije, JGEM (1997) Lincs: A linear constraint solver for molecular simulations. *J Comput Chem* 18:1463–1472.
3. Smith, PE, van Gunsteren, WF (1994) Consistent dielectric properties of the simple point charge and extended simple point charge water models at 277 and 300 k. *J Chem Phys* 100:3169–3174.
4. Ranganathan, R, Lu, KP, Hunter, T, Noel, JP (1997) Structural and functional analysis of the mitotic rotamase pin1 suggests substrate recognition is phosphorylation dependent. *Cell* 89:875–886.
5. Swope, WC, Pitera, JW, Suits, F (2004) Describing protein folding kinetics by molecular dynamics simulations: 1. theory. *J Phys Chem B* 108:6571–6581.
6. Schütte, C, Huisinga, W (2003) in *Handbook of Numerical Analysis*, eds Ciaret, PG, Lions, JL (North-Holland) Vol. X: Computational Chemistry, pp 699–744.
7. Weber, M (2003) Improved perron cluster analysis. *ZIB Report* 03-04.
8. Noé, F, Horenko, I, Schütte, C, Smith, JC (2007) Hierarchical Analysis of Conformational Dynamics in Biomolecules: Transition Networks of Metastable States. *J Chem Phys* 126:155102.
9. Norris, JR (1998) *Markov Chains*, Cambridge Series in Statistical and Probabilistic Mathematics (Cambridge University Press, Cambridge).
10. Metzner, P, Schütte, C, Vanden-Eijnden, E (2009) Transition Path Theory for Markov Jump Processes. *Multiscale Model Simul* 7:1192-1219.
11. Jäger, M, Nguyen, H, Crane, JC, Kelly, JW, Gruebele, M (2001) The folding mechanism of a beta-sheet: the ww domain1. *J Mol Biol* 311:373–393.
12. Singhal, N, Pande, VS (2005) Error analysis and efficient sampling in Markovian state models for molecular dynamics *J Chem Phys* 123:204909.
13. Noé, F (2008) Probability Distributions of Molecular Observables computed from Markov Models. *J Chem Phys* 128:244103.
14. van Gunsteren WF, Karplus M (1982) Effect of constraints on the dynamics of macromolecules *Macromolecules* 15:1528-1544
15. Feenstra KA, Hess B, Berendsen HJC (1999) Improving Efficiency of Large Time-scale Molecular Dynamics Simulations of Hydrogen-rich Systems J Comput Chem 20:786-798
16. Feenstra KA, Peter C, Scheek RM, van Gunsteren WF, Mark AE (2002) A comparison of methods for calculating NMR cross-relaxation rates (NOESY and ROESY intensities) in small peptides J Biomol NMR 23:182-194
17. Daura X, Mark AE, van Gunsteren WF (1998) Parametrization of aliphatic $_n$ united atoms of the GROMOS96 force field J Comput Chem 19:535-547